AIP | Journal of Applied Physics

Anomalous electrical transport properties of polyvinyl alcohol-multiwall carbon nanotubes composites below room temperature

G. Chakraborty, K. Gupta, A. K. Meikap, R. Babu, and W. J. Blau

Citation: J. Appl. Phys. **109**, 033707 (2011); doi: 10.1063/1.3544204
View online: http://dx.doi.org/10.1063/1.3544204
View Table of Contents: http://jap.aip.org/resource/1/JAPIAU/v109/i3
Published by the American Institute of Physics.

Anomalous electrical transport properties of polyvinyl alcohol-multiwall carbon nanotubes composites below room temperature

G. Chakraborty,[1] K. Gupta,[1] A. K. Meikap,[1,a)] R. Babu,[2] and W. J. Blau[2]
[1]*Department of Physics, National Institute of Technology, Durgapur Mahatma Gandhi Avenue, Durgapur, 713209 West Bengal, India*
[2]*Department of Physics, University of Dublin Trinity College, Dublin 2, Ireland*

(Received 29 September 2010; accepted 9 December 2010; published online 3 February 2011)

The dc and ac electrical transport property of polyvinyl alcohol-multiwall carbon nanotubes composites has been investigated within a temperature range $77 \leq T \leq 300$ K and in the frequency range 20 Hz–1 MHz in presence as well as in absence of a transverse magnetic field up to 1 T. The dc conductivity follows variable range hopping model. The magnetoconductivity of the samples changes a sign from positive to negative with an increase in temperature which can be interpreted by the dominancy of the quantum interference effect over the wave function shrinkage effect. The ac conductivity follows a power law whereas the temperature dependence of frequency exponent s can be explained by correlated barrier hopping model. The dielectric behavior of the samples has been governed by the grain and grain boundary resistance and capacitance. The ac conductivity reduces with the application of magnetic field. Although the theoretical model to explain it, is still lacking, we may conclude that this is due to the increase in grain and grain boundary resistance by the application of magnetic field. © *2011 American Institute of Physics*. [doi:10.1063/1.3544204]

I. INTRODUCTION

The unique structural, mechanical, electronic, and thermal properties of carbon nanotubes (CNTs) have made it an attractive material for nanoscience research.[1,2] They have potential application in electronic devices[3,4] and nanocomposites.[5,6] CNTs are ideal for reinforcement in composite materials since they have extraordinary properties like low density, high stiffness, and high strength.[7] Among the various composites with CNT as a reinforced material, polymer CNT composites have drawn a great attention due to its enhanced mechanical strength and enlarged electron transport properties.[8] Polyvinyl alcohol (PVA), on the other hand, is well known for its use as a matrix material for various inorganic composites. It is highly soluble in water and alcohol. So the PVA/CNT composites are easier to fabricate through water, alcohol, and surfactant medium.[4,9–15] The composites prepared in this way have a very high mechanical strength.[16,17] The aqueous dispersions of CNT require the presence of a surfactant like lithium or sodium dodecyl sulfate or cetyl trimethyl ammonium bromide (CTAB) due to its very low solubility in water. The dispersed CNT solution is added to PVA solution to make the PVA/CNT composite materials. There is no new bond established between the CNT and PVA matrix but the covalent linking between these two may increase the mechanical and other properties of this composites.[18] In the recent past, significant works have been done to explore the properties of PVA/CNT composites.[19–28] However most of them deal with the study of reinforcing CNT in PVA matrix or to find the mechanical properties of the composites. Very few works have been done to investigate the electrical properties of composite of PVA-multiwall carbon nanotubes (MWNT). Zhang *et al.*[29] investigated the electrical and dielectric properties of PVA-MWNT composites above room temperature. But the influence of magnetic field over the conductivity of such composites is ′not studied yet. This was the inspiration behind the present study of electron transport properties of PVA-MWNT composites below room temperature.

This work describes the synthesis and electrical transport properties of PVA-MWNT composites. To find the changes in the electrical property of PVA made by the MWNT, an extensive study is done to investigate the dc conductivity, dc magnetoconductivity, ac conductivity, dielectric properties and ac magnetoconductivity of the PVA-MWNT composites in the temperature range 77–300 K and in the frequency range 20 Hz–1 MHz with and without magnetic field.

II. SAMPLE PREPARATION AND EXPERIMENTAL TECHNIQUES

PVA, CTAB, MWNT (Nanocyl 3100), ethanol are collected from local market. Double distilled water is used for this investigation. Composites of PVA-MWNT are synthesized by *in situ* chemical oxidative polymerization. 1%, 3%, 5%, 7%, and 10% (by weight) MWNT solutions are prepared by dispersing MWNT in 120 mg of cationic surfactant CTAB and 1 M HCl solution with the help of a sonicator. It is then cooled down to 1–5 °C in ice chamber prior to use.

99%, 97%, 95%, 93%, and 90% (by weight) PVA solutions are prepared in a mixture of ethanol and water heating with continuous magnetic stirring at 80 °C. A clear transparent solution is obtained. This solution is then cooled to room temperature by stirring. 50 ml 99% PVA solution is mixed with 50 ml 1% MWNT solution under continuous magnetic stirring in an ice chamber. After 24 h, the mixture is taken in a petridish in an oven at 40 °C. A black film is obtained which is washed with water and ethanol several times. Fi-

a)Electronic mail: meikapnitd@yahoo.com.

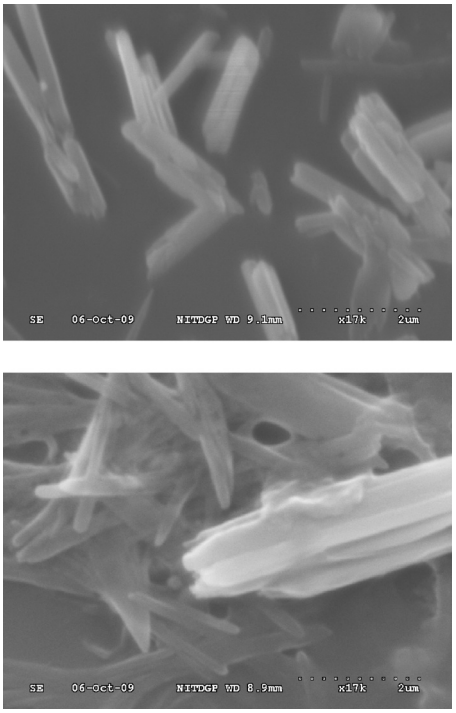

FIG. 1. SEM image of PVA-MWNT composites.

nally it is dried at 40 °C in an oven. For comparison pure PVA, PVA-CTAB samples are also prepared. Pure PVA is numbered as S_0, PVA+CTAB is taken as S_1. Sample containing 1 wt % MWNT is marked as S_2. Similarly, samples having 3%, 5%, 7%, and 10% MWNT content are considered as S_3, S_4, S_5, and S_6, respectively.

The x-ray diffraction (XRD) pattern is recorded using X'Pert pro x-ray diffractometer (PAN ANALYTICAL) with nickel filter Cu k_α radiation ($\lambda = 1.5414$ Å) in 2θ range from 10° to 80°. The electrical conductivity of the samples was measured by a standard four probe method after good contact was ensured with highly conducting graphite adhesive (Electrodag 5513, Acheson, Williston, VT) and fine copper wires as the connecting wires. The dc conductivity was measured with an 8(1/2)—digit Agilent 3458A multimeter. Conductivity that depends upon temperature was studied with a liquid nitrogen cryostat. For the control and measurement of the temperature, an ITC 502S Oxford temperature controller was used. For conductivity measurement, we cut the sample as a circular shape of diameter 1 cm from the film. The magnetoconductivity was measured in the same manner by the variation in the transverse magnetic field ($B < 1$ T) with an electromagnet.

III. RESULTS AND DISCUSSION

Figure 1 shows the scanning electron micrograph of PVA-MWNT samples. It is observed from the micrograph that CNTs are arranged parallel to each other. The composite samples show a columned growth in which the diameter of the PVA-MWNT composites has been increased, compared to that of pure MWNT.[30] Length of the tubes is in the range of 2–3 μm and diameter is in the range of 80–100 nm. This increase in diameter and columnar growth may be attributed

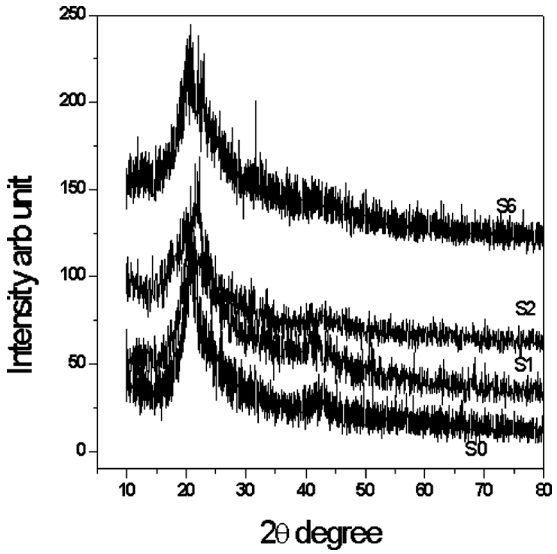

FIG. 2. XRD of PVA and PVA-MWNT composites.

to the uniform distribution of polymer on the surface of pure MWNT. Thus the scanning electron micrograph (SEM) images of the investigated samples give confirmation that in all the composite samples, MWNTs are coated by the polymer.

Figure 2 represents the XRD pattern of PVA-MWNT composites. Amorphous nature of the composite is obtained. Amorphous peak[31] of PVA is obtained at 20°. PVA-CTAB shows similar XRD spectrum to that of PVA. So it may be concluded that CTAB do not disturb the structure of the composite. XRD spectrum of pure MWNT has been indicated in the previous work with PANI-MWNT composites.[30] As the MWNTs are introduced in the PVA matrix, the peaks of PVA and MWNT almost coincide. As a result, peak broadening of XRD spectrums occurs.

To develop an idea regarding the effect of highly conducting CNTs in insulating PVA matrix, the direct current conductivity of all the samples have been measured in the temperature range 77–300 K. Figure 3 shows the room temperature conductivity ($\sigma_{300\ K}$) of all the samples with in-

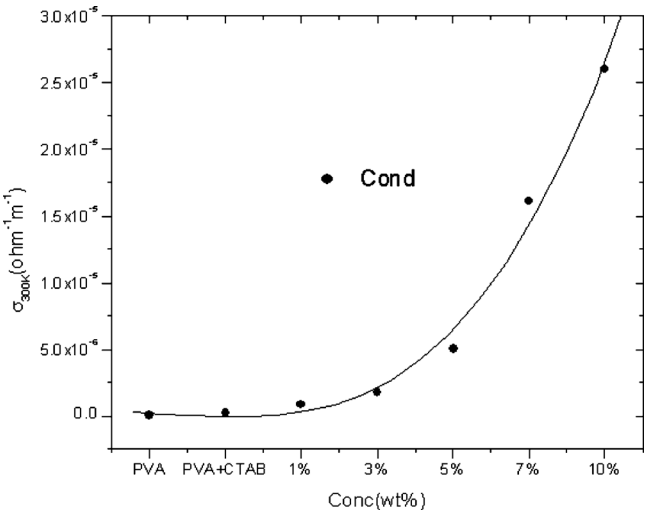

FIG. 3. Variation in room temperature conductivity with different concentration of PVA and PVA-MWNT composites.

TABLE I. Different physical parameters of samples: Conductivity at room temperature [σ(300 K)], Conductivity ratio (σ_r), temperature exponent (γ), Mott characteristic temperature ($T_{Mott,low}$) in the temperature range 77–150 K, Mott characteristic temperature ($T_{Mott,high}$) in the temperature range 150–300 K, localization length (L_{loc}), hopping length (R_{Hopp}), activation energy ($E_{a,low}$) at temperature range 77–150 K, activation energy ($E_{a,high}$) at temperature range 150–300 K, effective barrier height (W_H) and characteristic relaxation time (τ_0).

Parameters	S_0	S_1	S_2	S_3	S_4	S_5	S_6
σ(300 K) (Ω^{-1} m^{-1})	1.68×10^{-8}	1.52×10^{-7}	7.8×10^{-7}	1.77×10^{-6}	4.96×10^{-6}	1.60×10^{-5}	2.60×10^{-5}
σ_r	1326.53	622.56	37.01	30.67	13.35	12.63	5.54
γ	0.25	0.25	0.25	0.25	0.25	0.25	0.25
$T_{Mott,low}$ (K)	9.02×10^{6}	8.20×10^{6}	1.28×10^{6}	1.12×10^{6}	6.10×10^{5}	4.52×10^{4}	7.49×10^{3}
$T_{Mott,high}$ (K)	3.61×10^{8}	3.11×10^{8}	2.54×10^{8}	2.45×10^{8}	1.49×10^{8}	6.31×10^{7}	1.06×10^{7}
L_{loc} (nm)	2.42	2.65	2.77	2.89	3.02	3.40	4.01
R_{Hopp} (nm)	0.018	0.022	0.028	0.035	0.039	0.048	0.109
$E_{a,low}$ (eV)	0.114	0.158	0.293	0.359	0.373	0.554	0.563
$E_{a,high}$ (eV)	0.816	1.275	1.53	1.71	1.78	1.84	1.88
W_H (eV)	0.70	0.69	0.79	0.77	1.11	0.90	0.80
τ_0 (S)	9.50×10^{-13}	4.89×10^{-12}	9.02×10^{-14}	5.22×10^{-12}	2.83×10^{-13}	1.01×10^{-12}	1.27×10^{-13}

creasing content of CNT. Two samples of PVA and PVA with CTAB do not contain CNT but all the other shows the increasing content of CNT from 1% to 10%. It is observed from Fig. 3 that the increasing content of CNT have increased the conductivity of the samples by a significant amount. The conductivity ratio $\sigma_r(=\sigma_{300}/\sigma_{77})$ of different samples are also mentioned in Table I, which also increases with increasing CNT content in different samples. This increase in room temperature conductivity and resistivity ratio may be attributed to the incorporation of highly conducting CNTs into the insulating PVA matrix. Interaction of CNT and polymer structure of PVA increases the charge transfer process between them. It was reported earlier that the localization length (L_{loc}) of CNTs is around 10 nm (Ref. 32) for the presence of large π-conjugated structure whereas for pure PVA the localization length has been calculated as 2.72 nm. Thus, an enhancement in average localization length occurs in PVA-MWNT composites and this happens due to strong coupling between poorly conducting polymer and highly conducting MWNTs. The variation in conductivity of different samples with increasing temperature is shown in Fig. 4.

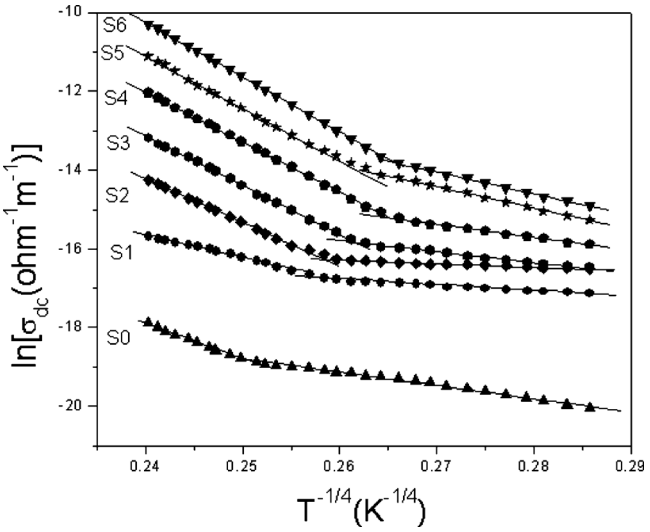

FIG. 4. Temperature dependence of the dc conductivity of PVA and different PVA-MWNT composites. The solid lines are fitted to Eq. (1).

It is observed in Fig. 4, up to 150 K, there is a very slight change in conductivity but beyond 150 K there is a rapid increase in conductivity. All the samples show semi conducting behavior which occurs due to the increase in charge transfer between PVA and CNT with the rise in temperature. This variation in conductivity with temperature can be explained in terms of Mott's variable range hopping (VRH) model.[33]

$$\sigma(T) = \sigma_0 \exp\left[-\left(\frac{T_{Mott}}{T}\right)^{\gamma}\right], \quad (1)$$

$$T_{Mott} = 24/[\pi K_B L_{loc}^3 N(E_F)], \quad (2)$$

where σ_0 is the conductivity at infinite temperature, T_{Mott} is the Mott characteristic temperature depending on the hopping barrier, electronic structure and energy distribution of the localized states, k_B is the Boltzmann constant, L_{loc} is the localization length, and $N(E_F)$ is the density of states at the Fermi level. The VRH exponent γ determines the dimensionality (d) by the relation $\gamma = 1/1+d$. The possible values of γ are 1/4, 1/3, and 1/2 for three-dimensional (3D), two-dimensional, and one-dimensional system, respectively. To have an idea of the mechanism of charge transport for the investigated samples, the temperature dependence of conductivity has been plotted in Fig. 4. A graph of $\ln[\sigma_{dc}(T)]$ versus $T^{-1/4}$ shows the presence of two different slopes. First slope indicates the linear variation in conductivity with temperature in the lower temperature range 77–150 K whereas the second slope indicates the same for higher temperature range 150–300 K. This linear temperature dependence of conductivity of all the samples indicates that the 3D charge transport is the dominating charge transport mechanism. The values of T_{Mott} for both the temperature range has been calculated from the slopes of the graph and indicated in Table I. For the lower temperature range, the value of T_{Mott} is quite small, but it becomes larger at higher temperature range. It is also observed that the values of T_{Mott} in both the temperature range decreases with increasing MWNT contents and this may due to increase in localization length. As the conducting islands due to MWNTs are present in between the insulating polymer matrix, the electronic wave functions extend in three-

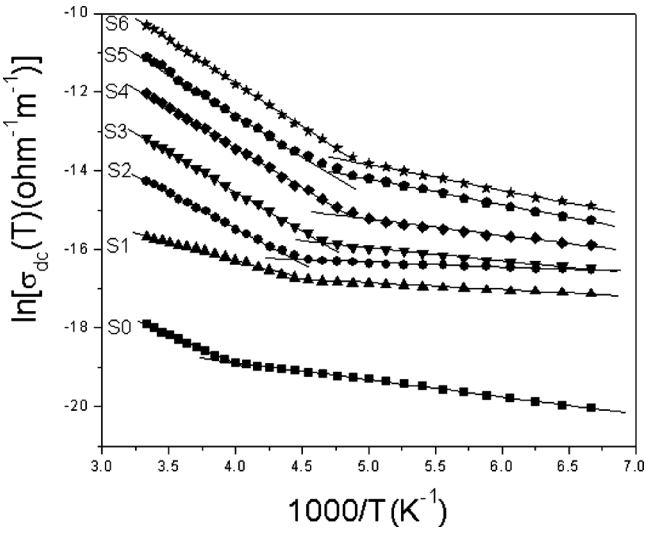

FIG. 5. Variation in the dc conductivity (σ_{dc}) with temperature of different PVA-MWNT composites. The solid lines are fitted to Eq. (3).

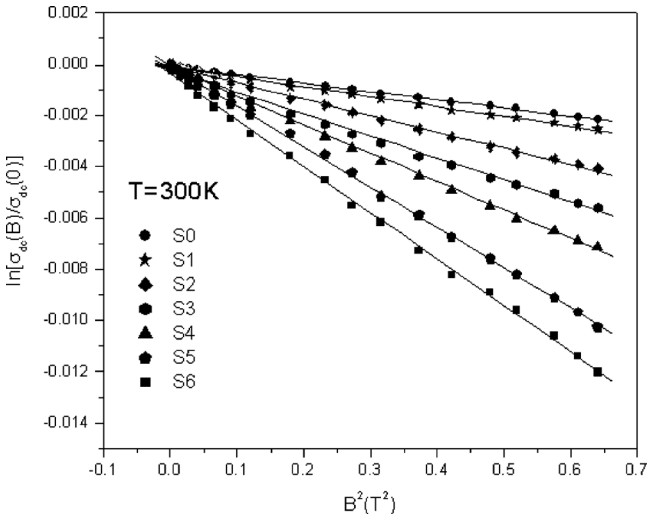

FIG. 6. Variation in the dc magnetoconductivity with perpendicular magnetic field of different PVA–MWNT at 300 K. The solid lines are fitted to Eq. (4).

dimension. As a result, 3D hopping of electrons occurs in the investigated samples. The existence of two different slopes becomes clearer by the study of activation behavior of the PVA-MWNT composites. The activation energy of all the investigated samples has been calculated by the Arrhenius equation

$$\sigma(T) = \sigma_0 \exp\left(-\frac{E_a}{K_B T}\right), \tag{3}$$

where σ_0 is the conductivity at infinite temperature, E_a is the activation energy, and k_B is the Boltzmann constant. E_a can be calculated from the slopes of the straight line plot of $\ln[\sigma(T)]$ with 1/T. Figure 5 shows the variation in $\ln[\sigma(T)]$ with 1000/T where two different activation regions for two different slopes are obtained for all the samples. The values of activation energy of all the samples at lower and higher temperature are indicated in Table I. At lower temperature range the activation energies are smaller in compare to higher temperature range. Thus, the interaction between MWNT and polymer becomes more prominent at higher temperature. It is also observed that the activation energy increases with the increase in CNT content. As the E_a of MWNT is large, the strong interaction of MWNT and the polymer results in larger activation energy for the PVA-MWNT composites. Thus, it may be concluded that, the CNT takes part in conduction mechanism at lower temperature but both CNT and polymer dominate the charge transport mechanism at the higher temperature range. Thus observed two slopes in conductivity versus temperature curve may be due to the above two charge transport mechanisms.

To find the influence of magnetic field of the conductivity of PVA-MWNT composites, the magnetoresistances of the samples were measured with increasing magnetic field up to 1 T and at different yet constant temperatures. Figure 6 shows the variation in magnetoconductivity with magnetic field at room temperature T=300 K. All the samples show negative magnetoconduction at room temperature. The measured data follow a simple phenomenological model consisting of two simultaneously acting hopping processes: the wave function shrinkage model[34,35] and the forward interference model.[36–38] According to wave function shrinkage model, the wave function of the electrons contract under the influence of magnetic field which results in a reduction in average hopping length and hence a negative magneto conductivity, i.e., conductivity decreases with increasing magnetic field. Under a small magnetic field, the magnetoconductivity ratio can be written as[34]

$$\ln\left(\frac{\sigma(B,T)}{\sigma(0,T)}\right) = -t_1 \frac{e^2 L_{loc}^4}{\hbar^2}\left(\frac{T_{Mott}}{T}\right)^{3/4} B^2, \tag{4}$$

where $t_1 = 5/2016$ and L_{loc} is the localization length. Again the forward interference model has the effect of forward interference among random paths in the hopping process between two sites spaced at a distance equal to optimum hopping distance, resulting in a positive magnetoconductivity. According to this model, the magneto conductivity ratio can be expressed as[36]

$$\frac{\sigma(B,T)}{\sigma(0,T)} = 1 + \frac{\frac{C_{sat}B}{B_{sat}}}{1+\frac{B}{B_{sat}}}, \tag{5}$$

where C_{sat} is a temperature dependent parameter and $B_{sat} = 0.7(h/e)(8/3)^{3/2}(1/L_{loc}^2)(T/T_{Mott})^{3/8}$. Due to the large localization length of CNT, the wave function shrinkage effect can't be observed in CNT. The earlier observation of magnetoconductivity of CNT was positive and interpreted in terms of quantum interference effect.[39,40] But the PVA-MWNT composites have a decreasing trend of magnetoconductivity with increasing magnetic field which may be due to the reduction in the localization length of MWNT by the insulating polymer matrix. Thus, there is a competition between the wave function shrinkage effect (negative magnetoconductivity) and the quantum interference effect (positive magnetoconductivity) which occur simultaneously to change the sign and magnitude of the magnetoconductivity. As the

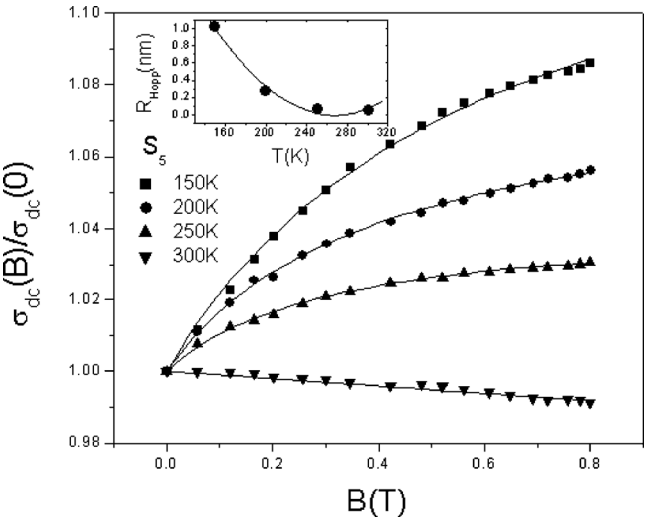

FIG. 7. Variation in the dc magnetoconductivity with perpendicular magnetic field of the sample S_5 at different temperatures. The solid lines are fitted to Eq. (5) at temperatures 150 K, 200 K, and 250 K and fitted to Eq. (4) at 300 K. Inset shows the variation in average hopping length (R_{Hopp}) with temperature.

experimental data at room temperature show a decreasing trend of magnetoconductivity with increasing magnetic field, so it may be concluded that the wave function shrinkage effect dominates over the quantum interference effect. So the measured data have been analyzed in terms of wave function shrinkage model. The variation in $\ln[\sigma(B,T)/\sigma(o/T)]$ versus B^2 is linear for different samples, as shown in Fig. 6. The points represent the experimental data and the lines represent the theoretical best fit in accordance with the wave function shrinkage model at low magnetic field. From Fig. 6 it is evident that the experimental data can be well described by the theory indicated by Eq. (4). From the slopes of the graph, the localization length has been calculated and is indicated in Table I. The localization length of different samples decreases with the increasing conductivity ratio. In general, the extent of disorder is expressed in terms of conductivity ratio. For higher disorder in the samples the electronic wave functions are localized into smaller regions resulting in a smaller localization length. So the localization length has an inverse relationship with conductivity ratio as well as the extent of disorder present in the sample. Thus, the localization length is strongly influenced by the disorder present in the sample. The average hopping length R_{Hopp} can be calculated from the relation

$$R_{Hopp} = (3/8)(T_{Mott}/T)^{1/4} L_{loc}. \quad (6)$$

The values of R_{Hopp} for different samples are indicated in Table I. Figure 7 shows the variation in magnetoconductivity of the sample S_5 at different temperature with various magnetic fields. As the temperature increases, the magnitude of the magnetoconductivity decreases and ultimately becomes negative at T=300 K, i.e., a change in sign in magnetoconductivity from positive to negative upon increasing the temperature can be noticed. All the samples show similar behavior. At lower temperature (where the MWNT is responsible for conduction), the enhancement of the average localization length of the composite is supported by the observed positive magnetoconductivity. But by increasing temperature, both MWNT and PVA are responsible for conduction process and the average localization length is reduced due to interaction between MWNT and PVA. As a result, the wave function shrinkage is dominated over quantum interference effect with increasing temperature which gives negative magnetoconductivity. In Fig. 7 the points represents the experimental data whereas the solid lines at temperatures 150, 200, 250 K are theoretical best fit obtained from Eq. (5) and from Eq. (4) at T=300 K. The figure reveals that the experimental data are in good accordance with the above mentioned theories. The localization lengths have been calculated from this analysis which varies from 26.32 to 3.04 nm with temperature increase from 150 to 300 K. The value of average hopping length has also been found from the known values of L_{loc} and T_{Mott} and with the help of Eq. (6). The variation in average hopping length with temperature is shown in the inset of Fig. 7. Thus the anomalous behavior of the PVA-MWNT composite sample shows a transformation from quantum interference effect to wave function shrinkage effect with increasing temperature.

The alternate current (ac) conductivity of the PVA-MWNT composites has been measured in the temperature range $77 \leq T \leq 300$ K and in the frequency range 20 Hz–1 MHz. The variation in conductivity with frequency at a particular temperature becomes predominant at higher frequency but at lower frequency, the conductivity is almost independent of frequency. In general many amorphous semiconductors or disordered systems have dc conductivity contribution (σ_{dc}) besides the ac conductivity. This may be the reason behind the frequency independence of conductivity at lower frequency region. The total conductivity at a particular temperature over a wide range of frequency obeys a power low with frequency, which can be expressed as[33,41,42]

$$\sigma'(f) = \sigma_{dc} + \sigma_{ac}(f) = \sigma_{dc} + \alpha f^s, \quad (7)$$

where σ_{dc} is the dc conductivity, α is the temperature dependent constant, and the frequency exponent $s \leq 1$. Upon subtracting the dc contribution from the total conductivity the frequency dependent contribution can be calculated. Figure 8 shows the linear variation in $\ln[\sigma_{ac}(f)]$ with $\ln[f]$ at different constant temperature for the sample S_2. All the other samples behave in a similar manner. This linear variation in $\ln[\sigma_{ac}(f)]$ with $\ln[f]$ shows that the frequency exponent "s" in Eq. (7) is independent of frequency. The value of s have been calculated from the slopes of the graphs of Fig. 8 for each temperature of different samples. The variation in s with temperature is shown in Fig. 9 for different samples. At lower temperature ($T < 150$ K), the value of s becomes almost temperature independent, but above $T > 150$ K, it decreases gradually with increasing temperature. In general, the nature of conduction process of disordered system is explained by two physical processes such as correlated barrier hopping (CBH) (Ref. 42) and quantum mechanical tunneling (electron tunneling,[43] small polaron tunneling,[42] and large polaron tunneling[41]). The nature of variation in s with temperature for different conduction process is different. So from the temperature variation in s, the exact nature of charge transport mechanism can be obtained. The frequency exponent s

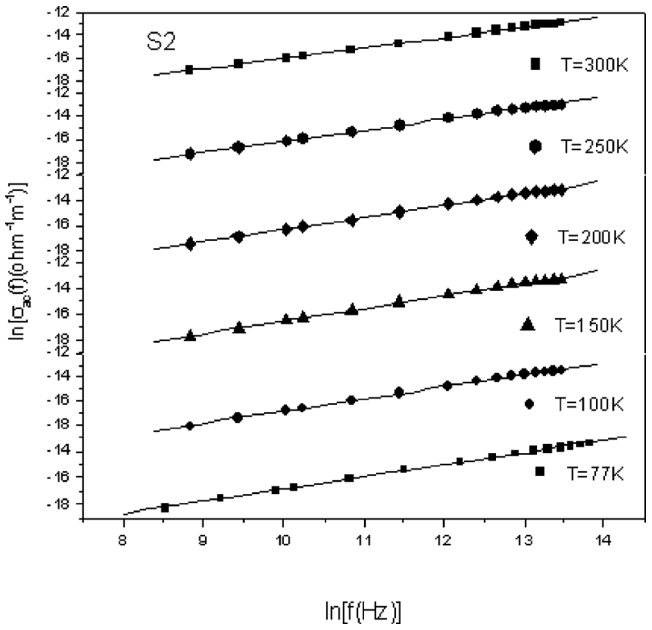

FIG. 8. Frequency dependence of ac conductivity of the sample S_2 at different temperatures.

becomes independent of temperature in electron tunneling theory whereas it increases with increasing temperature in small polaron theory and decreases at first and then increases with increasing temperature according to large polaron theory. But according to CBH model, there is only gradual decrease in s with increasing temperature. The trend of variation in s above T=150 K in the present investigated samples suggests that the CBH model is suitable for explaining the experimental data. CBH model suggests the hopping of the charge carriers between the sites over the potential barrier separating them and the frequency exponent s can be expressed as[42]

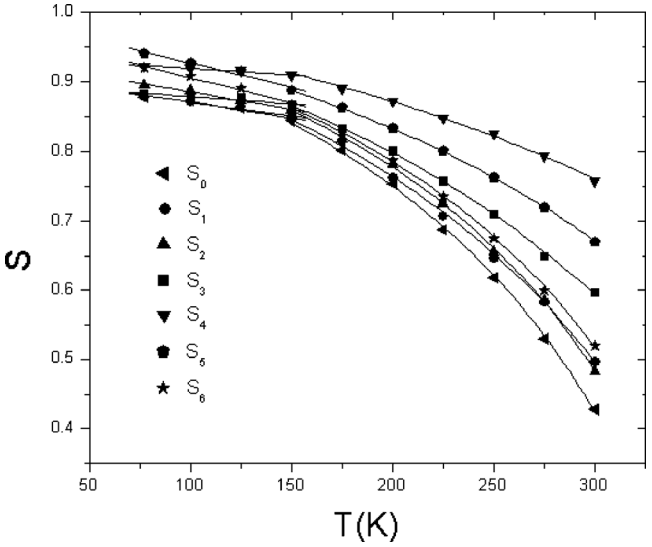

FIG. 9. The temperature variation in the frequency exponents "S" for different PVA-MWNT composites. The solid lines above 150 K are fitted to Eq. (8).

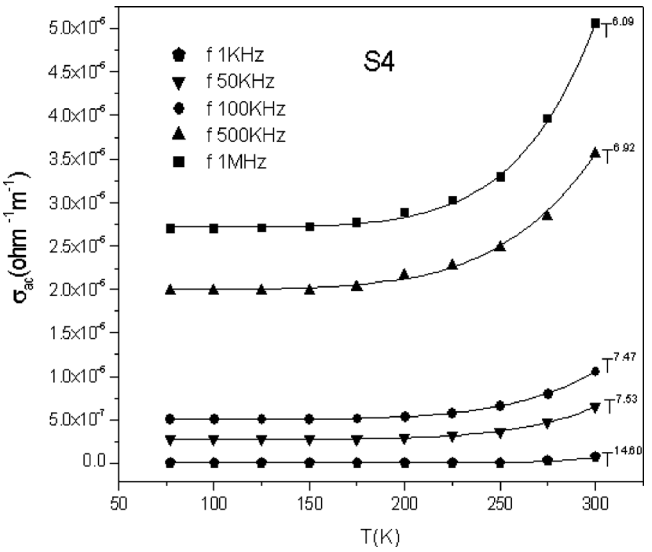

FIG. 10. AC conductivity as a function of temperature of the sample S_4 at different frequencies.

$$S = 1 - \frac{6k_BT}{W_H - k_BT\ln\left(\frac{1}{\omega\tau_0}\right)}, \quad (8)$$

where k_B, W_H, ω, and τ_0 are Boltzmann constant, effective barrier height, angular frequency, and characteristic relaxation time, respectively. According to Eq. (8), the variation in s with frequency becomes small for a large values of W_H/K_BT. Again in Fig. 8, the linear variation in σ_{ac} with frequency suggests that s is independent of frequency. So the experimental data has been analyzed with Eq. (8) as function of temperature keeping W_H and $\omega\tau_0$ as a fitting parameters. In Fig. 9, the points are the experimental data and solid lines represent the theoretical best fit obtained from Eq. (8) for different samples. The values of W_H and τ_0 at a fixed frequency of 10 kHz have been calculated and are enlisted in Table I. At lower temperature range where the value of W_H/K_BT becomes large, Eq. (8) transforms to a linear temperature dependency of s. Thus, the high value of W_H/K_BT at lower temperature may be the reason behind the linear temperature dependency of s. Thus, the trend of variation in s with temperature suggests that the charge transport mechanism of the investigated samples can be explained by the CBH model.

Figure 10 represents the variation in ac conductivity with temperature for the sample S_4 at different yet constant frequencies. At lower temperature (T < 150 K), a weak variation in ac conductivity with temperature can be noticed whereas this variation becomes larger at higher temperature (T > 150 K). The real part of complex ac conductivity is found to follow a power law $\sigma_{ac}(f) \propto T^n$. The points in Fig. 10 represents the experimental data whereas the solid line represents the best fit obtained by the above equation. The value of n has been obtained as a fitting parameter and is shown in Fig. 10. The value of "n" is strongly dependent on frequency for the sample S_4, the value of n varies from 14.60 to 6.09 with a frequency variation from 1 kHz to 1 MHz. According to the CBH model[42] the ac conductivity $\sigma'(f)$ is

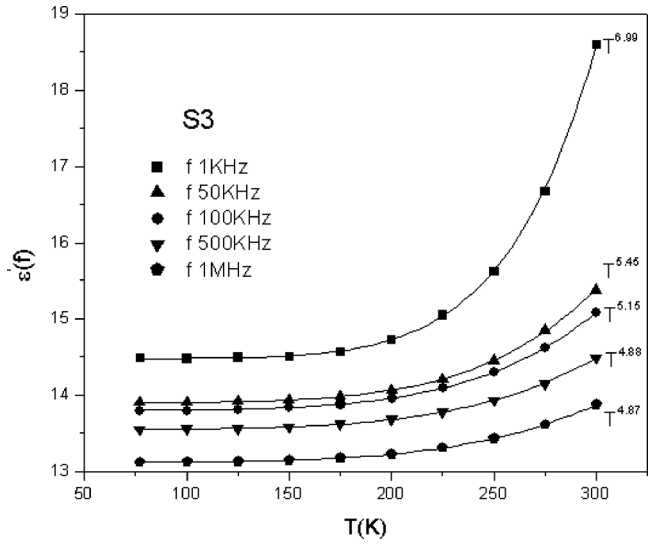

FIG. 11. Temperature variation in real part of permittivity of the sample S_3 at different frequencies.

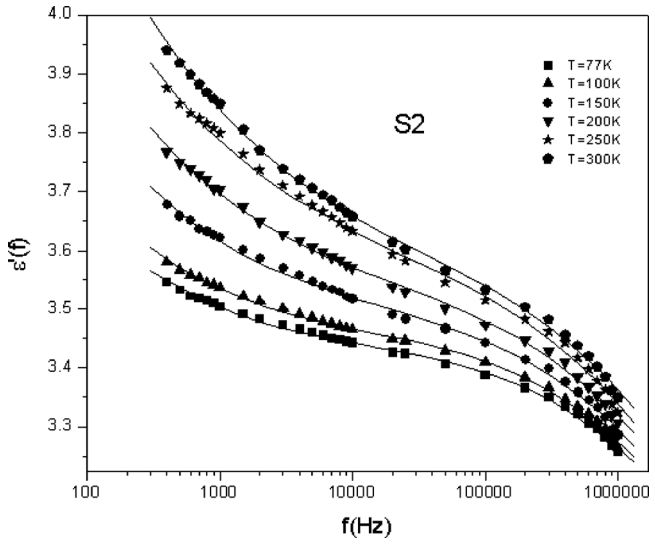

FIG. 12. Variation in dielectric constant as function of frequency at different temperatures of the sample S_2.

expressed as $\sigma'(f) \propto T^2 R_\omega^6$ [$\cong T^n$ with $n=2+(1-s)\ln(1/\omega\tau_0)$] for broad band limit and $\sigma'(f) \propto R_\omega^6 \cong T^n$ with $n=(1-s)\ln(1/\omega\tau_0)$ for narrow band limit, where $R_\omega = e^2/\{\pi\varepsilon\varepsilon_0[W_H - k_B T \ln(1/\omega\tau_0)]\}$. The theoretical values of n, has been calculated using broad band limit, taking $\tau_0 = 2.83 \times 10^{-13}$ S and the value of s=0.76 for 300 K and 0.92 for 77 K for different frequencies. The variation in the calculated values of n are in the range 6.84 to 5.18 for 300 K and 3.61 to 3.06 for 77 K for broad band limit and 4.84 to 5.18 for 300 K and 1.61 to 1.06 for 77 K for narrow band limit with frequency variation from 1 kHz to 1 MHz. The experimental values are not close to the theoretical values obtained from broad band limit and narrow band limit, i.e., there is a discrepancy between theoretical and experimental result. Anyway, more studies are necessary to formulate the true mechanisms.

Figure 11 shows the temperature dependence of real part of dielectric permittivity of $\varepsilon'(f)$ for the sample S_3 for different yet constant frequencies. In the figure there is no sharp peak up to T=300 K, which is the maximum possible temperature in the present investigation. At constant frequencies, the real part of dielectric permittivity increases with temperature following a power law $\varepsilon'(f) \propto T^n$. In the figure the points are the experimental data and the solid lines represent the best possible fitting according to the power law. Values of n have been calculated from the power law fitting and are mentioned in the figure. The value of n depends on the frequency and its value decreases with increasing frequency for all the samples. Thus, a larger variation in the $\varepsilon'(f)$ with temperature is observed at lower frequency compared to the higher frequency. In general, interfacial polarization is exhibited by disordered semiconductors due to structural inhomogenities and existence of free charges. At low frequencies, the hopping electron may be trapped by the inhomogenities. As the resistance of the composites decreases with increasing temperature, there is an increase in $\varepsilon'(f)$ with temperature at a particular frequency. Electron hopping is promoted by the low resistance and hence a larger polarizability or larger $\varepsilon'(f)$ results occurred. The variation in $\varepsilon'(f)$ with frequency has also been studied for all the composites at different temperature and are shown in Fig. 12 for the sample S_2 at different yet constant temperatures. At a fixed temperature, there is a sharp increase in $\varepsilon'(f)$ at lower frequency. This may occur due to the presence of large degree of dispersion caused by the charge transfer within the interfacial diffusion layer present between the electrodes. The magnitude of dielectric dispersion depends on the temperature. At lower temperature, the electric dipoles freeze easily through the relaxation process due to which there exists decay in polarization with respect to the applied electric field. As a result, a sharp decrease in $\varepsilon'(f)$ at lower frequency region can be observed. At higher temperature there is a quick rate of polarization and hence relaxation occurs at higher frequency. Thus the inhomogeneous nature of the samples containing different permittivity and conductivity regions governs the frequency behavior of $\varepsilon'(f)$ where the poorly conducting region blocks the charge carriers. Maxwell–Wagner capacitor model[44–46] can explain the effective dielectric of such inhomogeneous system. The complex impedance of inhomogeneous system is compared with an ideal equivalent circuit having resistance and capacitance due to grain and interfacial grain boundary contribution, according to which

$$Z = \frac{1}{i\omega C_0 \varepsilon(\omega)} = Z' - iZ'', \tag{9}$$

$$Z' = \frac{R_g}{1+(\omega R_g C_g)^2} + \frac{R_{gb}}{1+(\omega R_{gb} C_{gb})^2}, \tag{10}$$

$$Z'' = \frac{\omega R_g^2 C_g}{1+(\omega R_g C_g)^2} + \frac{\omega R_{gb}^2 C_{gb}}{1+(\omega R_{gb} C_{gb})^2}, \tag{11}$$

where the subindexes "g" and "gb" represents the grain and interfacial grain boundary, respectively, R=resistance, C=capacitance, $\omega = 2\pi f$, and C_0=free space capacitance. The real part of the complex impedance for all the samples have been calculated by the relation

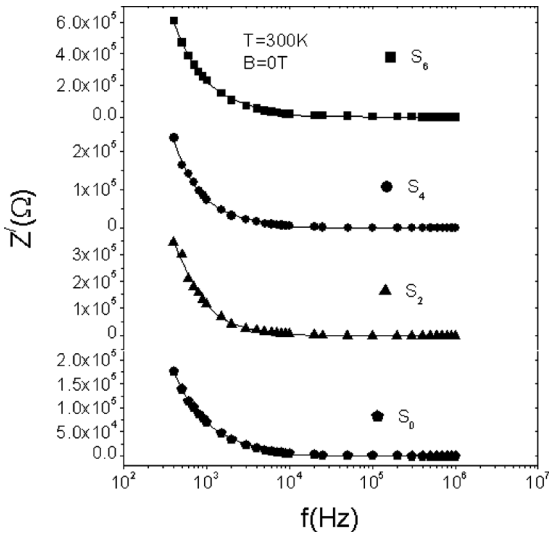

FIG. 13. The real part of the complex impedance vs frequency at T =300 K of different PVA-MWNT composites. The solid lines are fitted to Eq. (10).

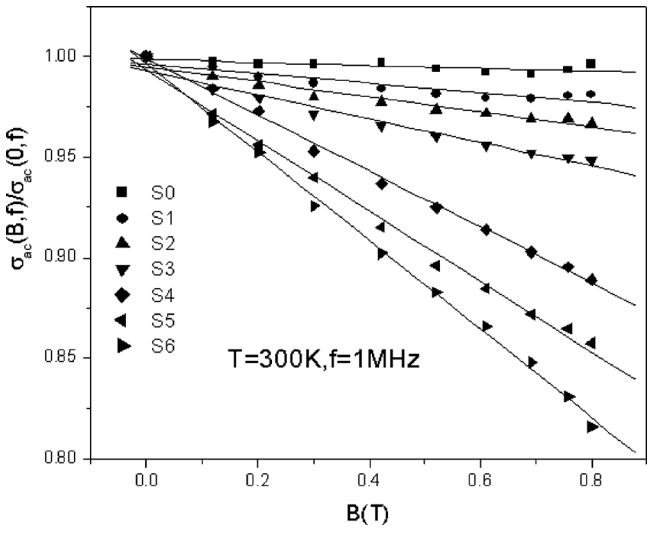

FIG. 14. Magnetic field dependence of the ac conductivity of different PVA-MWNT composite at 300 K and constant frequency 1 MHz.

$$Z'(f) = \frac{\varepsilon''(f)}{\omega C_0[\varepsilon'(f)^2 + \varepsilon''(f)^2]}, \quad (12)$$

where $\varepsilon'(f)$ and $\varepsilon''(f)$ are the real and imaginary part of dielectric permittivity, respectively. The real part of complex impedance has been analyzed by Eq. (10). The frequency variation in real part of the complex impedance of different samples is shown in Fig. 13 at T=300 K. The points in Fig. 13 represent the experimental data whereas the solid lines represent the theoretical best fit obtained from Eq. (10). The grain and grain boundary resistance and capacitance have been evaluated from the fitting and at T=300 K the values lie in the range 0.018–1.17 MΩ for R_g, 0.42–1.40 nF for C_g, 0.33–75 MΩ for R_{gb} 0.06–1.43 nF for C_{gb} for different samples. The figure shows that the experimental data is well fitted with the theory. From the values of grain and grain boundary resistance, it is clear that, the grain boundary resistance is much greater than that of grain resistance. Thus it may be concluded that, the grain boundary contribution dominated over the grain contribution.

The magnetic field variation in the real part of ac conductivity for different samples at room temperature and frequency f=1 MHz is shown in Fig. 14. The conductivity of all the samples decreases with increasing magnetic field. At present, the direct explanation of the behavior of ac conductivity under the influence of magnetic field is not available. But the dielectric property of these systems can be explained in terms of grain and grain boundary resistance and capacitances. The relation between the real part of ac conductivity and the dielectric response can be written by the relation $\sigma'(B,f) = \omega\varepsilon_0\varepsilon''(B,f)$. As the value of $\varepsilon''(f)$ is dependent on grain and grain boundary resistance and capacitance, the ac conductivity can be written as[47]

$$\sigma'(B,f) = \frac{d}{A(R_g + R_{gb})} \frac{1 - \omega^2\tau_g\tau_{gb} + \omega^2\tau(\tau_g + \tau_{gb})}{1 + \omega^2\tau^2}, \quad (13)$$

where $\tau_g = C_g R_g$, $\tau_{gb} = C_{gb} R_{gb}$, and $\tau = R_g R_{gb}(C_g + C_{gb})/(R_g + R_{gb})$. If the magnetic field changes any of the values of these resistances, the ac conductivity will change. It will be clearer if we analyze the real part of complex impedance with frequency under the influence of magnetic field. Figure 15 shows the variation in complex impedance with frequency in absence (B=0 T) and in presence (B=0.8 T) of magnetic field of different samples. The data have been analyzed by using the Eq. (10) and evaluated the grain and grain boundary contribution in absence and in presence of magnetic field. It is seen from analysis that change in the order of magnitude of grain and grain boundary capacitance under magnetic field is very small in compare to the change in the grain and grain boundary resistances. The value of grain and grain boundary resistance increases with increasing magnetic field for all the samples. Hence, the total contribution due to grain and grain boundary resistance ($R = R_g + R_{gb}$) varies from 3.66×10^5 to 7.51×10^7 Ω in absence of magnetic field and 1.20×10^6 to 4.28×10^8 Ω in presence of magnetic field

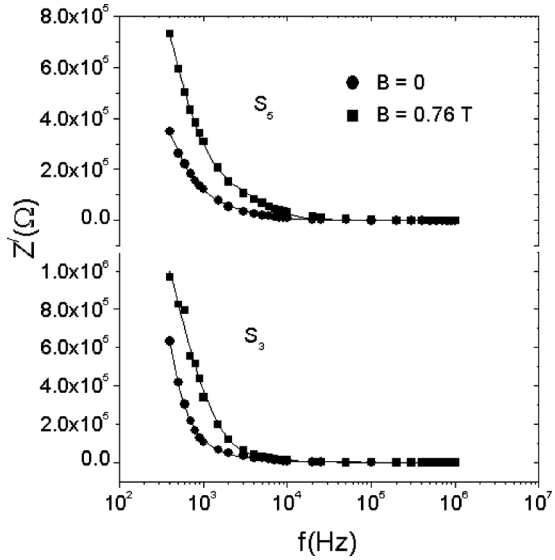

FIG. 15. The frequency dependence of the real part of the complex impedance at 300 K of the samples S_3 and S_5 with and without magnetic field. The solid lines are fitted to Eq. (10).

B=0.8 T for different samples. Thus the applied magnetic field has an effect on the grain and grain boundary resistance and hence the observed reduction in ac conductivity in Fig. 14 may be due to increase in $R=R_g+R_{gb}$ by increasing magnetic field. But as the theoretical expression for magnetic field dependency of grain and grain boundary behavior is still lacking, the experimental results can't be compared with the theory directly. Thus to find the true mechanism of the magnetic field dependent ac conductivity, a more rigorous theoretical and experimental work is needed.

IV. CONCLUSION

The dc conductivity of all the samples follows a simple hopping type of charge conduction mechanism. At lower temperature, there is a very weak variation in dc conductivity with temperature but the variation becomes larger beyond $T>150$ K. Two different excitation energy was calculated to explain such temperature dependence of dc conductivity. The dc magnetoconductivity of all the samples were negative at room temperature and can be explained in terms of wave function shrinkage effect. Magnetoconductivity of all the samples changes a sign from positive to negative with the increase in temperature from 150 to 300 K, which happens due to decrease in the localization length and thus transformation from quantum interference effect to wave function shrinkage effect. The real part of ac conductivity follows a power law given by $\sigma'(f)\infty f^S$ The temperature dependence of universal dielectric responses is found to follow CBH charge transfer mechanism. The variation in ac conductivity and dielectric permittivity with temperature for all samples follow the equations $\sigma'(f)\infty T^n$ and $\varepsilon'(f)\infty T^n$ where the value of n is found to be strongly dependent on frequency. The real part of complex permittivity shows a large degree of dispersion at lower frequency which is interpreted in terms of Maxwell-Wagner capacitor model. The contribution due to grain resistance is smaller than that of grain boundary resistance. The total resistance due to grain and grain boundary increases under the influence of magnetic field.

ACKNOWLEDGMENTS

The authors gratefully acknowledge the principal assistance received from the MHRD, Government of India during this work.

[1]C. N. R. Rao, B. C. Satishkumar, A. Govindaraj, and M. Nath, ChemPhysChem **2**, 78 (2001).
[2]R. H. Baughman, A. Zakhidov, and W. A. de Hee, Science **297**, 787 (2002).
[3]J. Sandler, M. S. P. Shaffer, T. Prasse, W. Bauhofer, K. Schulte, and A. N. Windle, Polymer **40**, 5967 (1999).
[4]A. B. Dalton, S. Collins, E. Munoz, J. M. Razal, V. H. Ebron, J. P. Ferraris, J. N. Coleman, B. G. Kim, and R. H. Baughman, Nature (London) **423**, 703 (2003).
[5]S. Fan, M. G. Chapline, N. R. Franklin, T. W. Tombler, A. M. Cassell, and H. Dai, Science **283**, 512 (1999).
[6]A. Modi, N. Koratkar, E. Lass, B. Wei, and P. M. Ajayan, Nature (London) **424**, 171 (2003).
[7]X. Wang, S. Y. Park, K. H. Yoon, W. S. Lyoo, and B. G. Min, Fibers Polym. **7**, 323 (2006).
[8]A. L. Martínez-Hernández, C. Velasco-Santos, and V. M. Castaño, in *Chemistry of Carbon Nanotubes*, edited by V. A. Basiuk and E. V. Basiuk (American Scientific, Stevenson Ranch, CA, 2008), Vol. 2, Chap. 8.
[9]A. G. Rozhin, Y. Sakakibara, H. Kataura, S. Matsuzaki, K. Ishida, Y. Achiba, and M. Tokumoto, Chem. Phys. Lett. **405**, 288 (2005).
[10]X. F. Zhang, T. Liu, T. V. Sreekumar, S. Kumar, X. D. Hu, and K. Smith, Polymer **45**, 8801 (2004).
[11]X. Zhang, T. Liu, T. V. Srekumar, S. Kumar, V. C. Moore, R. H. Hauge, and R. E. Smalley, Nano Lett. **3**, 1285 (2003).
[12]M. S. P. Shaffer and A. H. Windle, Adv. Mater. **11**, 937 (1999).
[13]A. G. Rozhin, Y. Sakakibara, M. Tokumoto, H. Kataura, and Y. Achiba, Thin Solid Films **464–465**, 368 (2004).
[14]A. Chatterjee, Fibers Polym. **3**, 134 (2002).
[15]S. H. Kim, B. G. Min, and S. C. Lee, Fibers Polym. **6**, 108 (2005).
[16]B. Vigolo, P. Poulin, M. Lucas, P. Launois, and P. Bernier, Appl. Phys. Lett. **81**, 1210 (2002).
[17]A. B. Dalton, S. Collins, J. Razal, E. Munoz, V. H. Ebron, B. G. Kim, J. N. Coleman, J. P. Ferraris, and R. H. Baughman, J. Mater. Chem. **14**, 1 (2004).
[18]E. V. Basiuk, A. Anis, S. Bandyopadhyay, E. Alvarez-Zauco, S. L. I. Chan, and V. A. Basiuk (2008).
[19]L. Liu, A. H. Barber, S. Nuriel, and H. D. Wagner, Adv. Funct. Mater. **15**, 975 (2005).
[20]A. B. Dalton, C. Stephan, J. N. Coleman, B. McCarthy, P. M. Ajayan, S. Lefrant, P. Bernier, W. J. Blau, and H. J. Byrne, J. Phys. Chem. B **104**, 10012 (2000).
[21]A. Star, J. F. Stoddart, D. Steuerman, M. Diehl, A. Boukai, E. W. Wong, X. Yang, S.-W. Chung, H. Choi, and J. R. Heath, Angew. Chem., Int. Ed. **40**, 1721 (2001).
[22]M. J. O'Connell, P. Boul, L. M. Ericson, C. Huffman, Y. Wang, E. Haroz, C. Kuper, J. Tour, K. D. Ausman, and R. E. Smalley, Chem. Phys. Lett. **342**, 265 (2001).
[23]R. J. Chen, Y. Zhang, D. Wang, and H. Dai, J. Am. Chem. Soc. **123**, 3838 (2001).
[24]J. Chen, H. Liu, W. A. Weimer, M. D. Halls, D. H. Waldeck, and G. C. Walker, J. Am. Chem. Soc. **124**, 9034 (2002).
[25]R. Ramasubramaniam, J. Chen, and H. Liu, Appl. Phys. Lett. **83**, 2928 (2003).
[26]H. Xia, Q. Wang, and G. Qiu, Chem. Mater. **15**, 3879 (2003).
[27]Y. Sabba and E. L. Thomas, Macromolecules **37**, 4815 (2004).
[28]J. Chen, R. Rajagopal, C. H. Xue, and H. Y. Liu, Adv. Funct. Mater. **16**, 114 (2006).
[29]J. Zhang, M. Mine, D. Zhu, and M. Matsuo, Carbon **47**, 1311 (2009).
[30]G. Chakraborty, S. Ghatak, A. K. Meikap, T. Woods, R. Babu, and W. J. Blau, J. Polym. Sci., Part B: Polym. Phys. **48**, 1767 (2010).
[31]J. Bhadra and D. Sarkar, Indian J. Pure Appl. Phys. **48**, 425 (2010).
[32]J. Joo, S. M. Long, J. P. Pouget, E. J. Oh, A. G. MacDiarmid, and A. J. Epstein, Phys. Rev. B **57**, 9567 (1998).
[33]N. F. Mott and E. Davis, *Electronic Process in Noncrystalline Materials*, 2nd ed. (Clarendon, Oxford, 1979).
[34]B. I. Shklovskii, Sov. Phys. Semicond. **17**, 1311 (1983).
[35]B. I. Shklovskii and A. L. Efros, *Electronic Properties of Doped Semiconductors* (Springer, Berlin, 1984), p. 202.
[36]V. L. Nguyen, B. Z. Spivak, and B. I. Shklovskii, Sov. Phys. JETP **62**, 1021 (1995).
[37]U. Sivan, O. Entin-Wohiman, and Y. Imry, Phys. Rev. Lett. **60**, 1566 (1988).
[38]R. Rosenbaum, A. Milner, S. Hannens, T. Murphy, E. Palm, and B. Brandt, Phys. B **294–295**, 340 (2001).
[39]M. S. Fuhrer, W. Holmes, P. L. Richards, P. Delaney, S. G. Louie, and A. Zettl, Synth. Met. **103**, 2529 (1999).
[40]Y. Yosida and I. Oguro, J. Appl. Phys. **86**, 999 (1999).
[41]A. R. Long, Adv. Phys. **31**, 553 (1982).
[42]S. R. Elliott, Adv. Phys. **36**, 135 (1987).
[43]A. L. Efros, Philos. Mag. B **43**, 829 (1981).
[44]J. C. Maxwell, *A Treatise on Electricity and Magnetism* (Oxford University Press, Oxford, 1988), Vol. 1.
[45]K. W. Wagner, Ann. Phys. **40**, 53 (1913).
[46]V. Hippel, *Dielectrics and Waves* (Wiley, New York, 1954).
[47]G. Catalan, Appl. Phys. Lett. **88**, 102902 (2006).